Journal of the Brazilian Society of Mechanical Sciences and Engineering (2026) 48:171
https://doi.org/10.1007/s40430-025-06168-7

TECHNICAL PAPER

Methodology for tunnel inspection using drone with autonomous navigation

Leandro Silva de Assis[1] · Antonio Carlos Daud Filho[2] · Lidia Gianne Souza da Rocha[3] · Kelen Cristiane Teixeira Vivaldini[3] · Glauco Augusto de Paula Caurin[4] · Marcos Massao Futai[1]

Received: 16 July 2025 / Accepted: 12 November 2025

Abstract

A methodology is presented for the digital reconstruction of an underground tunnel geometry using UAV photogrammetry, which is first tested in a computer simulation environment using the MRS UAV System, the Robot Operating System (ROS), and the Gazebo open-source robotics simulator. An algorithm for UAV navigation inside the tunnel is proposed, aiming to maintain a centralized position relative to the walls, ceiling, and floor. The proposed navigation algorithm can be used in a tunnel environment with few obstacles and overhanging structures, characterized by a practically constant cross-section along its entire length, which renders localization algorithms that utilize LiDAR scanning and point clouds impractical. These characteristics are common to rail or road transport tunnels. The methodology is tested in a computer simulation, and photogrammetry results showed that it is possible to digitally reconstruct the reference underground tunnel and faithfully reproduce details in texture, shape, and color. Thus, experiments were carried out in sections of a highway tunnel under construction to apply the same methodology for reconstructing three-dimensional geometry using photogrammetry, the images of which come from cameras onboard a drone with autonomous navigation using the same algorithm. The quantitative evaluation revealed a cross-sectional area difference of 0.21% between the designed area (70.72 m^2) and the area obtained from the photogrammetric model (70.57 m^2), confirming the high precision. Qualitatively, the model effectively represented textures and colors, validating the methodology for real-world applications.

Keywords Tunnel inspection · Geometry reconstruction · UAV autonomous navigation · Photogrammetry · Simulation

Technical Editor: Marco Antonio Meggiolaro.

✉ Antonio Carlos Daud Filho
antonio.daud.filho@usp.br

Leandro Silva de Assis
leandroassis@usp.br

Lidia Gianne Souza da Rocha
lidiagianne@gmail.com

Kelen Cristiane Teixeira Vivaldini
vivaldini@ufscar.br

Glauco Augusto de Paula Caurin
gcaurin@usp.br

Marcos Massao Futai
futai@usp.br

[1] Department of Structural and Geotechnical Engineering, Polytechnic School, University of São Paulo, Av. Prof. Almeida Prado, 83, São Paulo, São Paulo 05508-070, Brazil

[2] Department of Mechatronics and Mechanical Systems Engineering, Polytechnic School, University of São Paulo, Av. Professor Mello Moraes, 2231, São Paulo, São Paulo 05508-030, Brazil

[3] Department of Computer, Federal University of São Carlos, Rod. Washington Luís, Km 235, São Carlos, São Paulo 13565-905, Brazil

[4] Department of Aeronautical Engineering, São Carlos School of Engineering, University of São Paulo, Av. João Dagnone, 1100, São Carlos, São Paulo 13566-590, Brazil

Published online: 11 February 2026

1 Introduction

The aging of underground infrastructures can lead to degradation and collapse, incurring high costs for operating companies. Moreover, repairs can be time-consuming and expensive. In the case of tunnel collapses, examples include the collapse of the suspended roof for air ventilation onto traffic in the Sasago Tunnel of the Chuo Expressway near Tokyo, on December 2, 2012, causing nine deaths [1], and a rockfall at the Hanekleiv tunnel, Norway, in December 2006 [2]. The result of the collapse is shown in Fig. 1. Therefore, to prevent the collapse of these structures, appropriate management, inspection, and maintenance strategies should be applied.

The first aspect of tunnel inspection is identifying the types of degradation that may affect the tunnels and performing the necessary maintenance. In structural concrete tunnels, the defects include scaling, cracking (transverse, longitudinal, horizontal, vertical, diagonal, pattern, d-cracks, random), spalling, joint spall, pop-outs, efflorescence, staining, delamination, honeycomb, water leakage, salt accumulation, frost damage, and rust. These degradations must be detected early to ensure the longevity and safety of the infrastructure [3]. This information could further reveal a tunnel structural deformation and other health issues [4].

Tunnel inspection is traditionally performed by staff conducting a visual inspection or using inspection equipment, walking the underground route [5]. Another recent alternative is the inspection using Unmanned Ground Vehicles (UGVs), which can be legged robots, crawlers, or rail cars [6] that run along the path of the rails in train tunnels. UGVs can carry substantial payloads (5–10 kgs) and operate for extended periods (a few hours). However, they offer high-resolution sensing with a smaller field of view and lower coverage speed than unmanned aerial vehicles (UAVs). These, in turn, can approach points distant from the ground for image taking and data acquisition, such as ceiling walls. They are also more susceptible to obstacles, occlusions, and other sensing limitations [7]. In some tunnels, there is no possibility of ground traffic, either due to the inconsistency of the platform or due to the accumulation of mud. In this context, underground tunnel inspection activities can profit from using unmanned aerial vehicles (UAVs) equipped with onboard sensors, such as RGB, thermal, multispectral cameras, profilometers, and LiDAR scan systems, to facilitate quick inspections.

Inspecting the underground tunnel also involves checking its geometry. Thus, the 3D (three-dimensional) model reconstruction makes this inspection feasible. A 3D geometric infrastructure model can be constructed from point cloud data collected from the drone's onboard sensors, which can be integrated into digital platforms, creating a Digital Twin. From this, a virtual replica of the physical asset facilitates real-time monitoring and management throughout the tunnel lifecycle [8].

Photogrammetry, a widely used technique for 3D model reconstruction, can also be applied to create this virtual model. It involves obtaining reliable information from images and other systems or sensors without direct physical contact with the object [9]. Using drones in aerial photogrammetry has proven highly effective for inspecting urban infrastructure assets. The lack of Global Navigation Satellite System (GNSS) signals in confined spaces, such as tunnels, presents a significant challenge, making it difficult to control the drone's trajectory. In GPS-denied environments, drone navigation relies entirely on onboard sensors, requiring advanced perception, mapping, localization, obstacle avoidance, and path planning techniques [10]. The poor lighting conditions obscure key points of interest in the images, hindering the creation of an accurate three-dimensional model.

Autonomously flying the UAV through the tunnel would also offer advantages over manually controlling it. The accuracy and resolution of captured images can be enhanced by the UAV's ability to fly at optimal heights and maintain precise positions. This capability is crucial for 3D reconstruction, leading to more detailed and accurate models than those generated by manually piloted drones [11].

Fig. 1 Examples of tunnel collapses: (**a**) collapse of suspended roof for air ventilation in the Sasago Tunnel of the Chuo Expressway near Tokyo, on December 2, 2012 [1]. (**b**) rock fall at the Hanekleiv tunnel in Norway, in December 2006 [2]

The advanced integration of path planning algorithms into autonomous drones enhances the efficiency of data collection for creating 3D models. These algorithms optimize the image collection rate to ensure sufficient stereoscopy for 3D reconstruction while minimizing the volume of irrelevant data collected.

Autonomous UAV navigation in tunnels requires control algorithms that can safely guide the vehicle while maintaining a central position relative to the surrounding surfaces. These algorithms rely on onboard sensors to measure distances to the walls, ceiling, and floor, ensuring obstacle avoidance and stable flight along the tunnel axis. Navigation methods are commonly divided into three categories: mapless, map-building, and map-based approaches [12]. Mapless navigation relies on real-time perception without prior maps, utilizing features extracted from the environment to guide motion. Map-building approaches generate maps on the fly, typically using simultaneous localization and mapping (SLAM) to support localization and path planning. In contrast, map-based strategies assume a known layout, allowing the UAV to plan paths and detours more globally.

In GPS-denied and visually constrained environments such as tunnels, UAVs frequently rely on SLAM-supported or map-based methods that fuse onboard sensor data to estimate position and avoid obstacles [12]. However, the effectiveness of these techniques can degrade in feature-sparse or poorly lit settings, where visual odometry becomes unreliable and drift accumulates [13]. Such limitations are particularly detrimental in scenarios that require precise and consistent localization, such as infrastructure inspection and 3D reconstruction. One way to obtain location in underground environments without GPS is to use a wireless location system based on ultra-wideband (UWB) technology. This consists of positioning fixed antennas (anchors) at known coordinates throughout the underground environment and a mobile antenna onboard the UAV. By measuring the distances between the mobile antenna and the fixed antennas, the UAV's position can be estimated using algorithms such as the least squares method [14]. However, particularly in the underground tunnel environment, signals from this system can suffer from line-of-sight obstructions, as well as problems due to the signal traveling through multipaths, degrading, or failing to estimate the position [15].

In [16], the authors propose a method for tunnel navigation based on measurements from a depth camera. Still, this method is only suitable for tunnels with many curves and a small diameter. In wide, long, and straight tunnels, the depth distance measurements taken in front of the UAV are faulty or exceed the sensor's maximum range. Another possible strategy presented in [17] involves using cameras to identify and track lines drawn on the ground that indicate the path to be followed. This approach is viable for autonomous navigation in well-lit tunnels that require frequent inspection, as it allows for precise targeting of the point where the line was drawn. However, the presence of dirt could cover and hide the line.

Many underground tunnels have a geometry with a virtually constant cross-section along their entire length, as well as no bifurcations–that is, they have only one long and continuous section with few or no curves–and few obstacles or overhanging structures, in addition to feature-sparse and poor lighting, and a wide cross-section. These are common characteristics of rail or road tunnels. The combination of these characteristics makes it challenging to obtain odometry, i.e., positioning and speed during flight, using algorithms based on point clouds, depth cameras, and visual odometry. Therefore, in these environments, the application of map-based navigation algorithms, such as SLAM-based ones, is impractical. Thus, navigation algorithms more appropriate for these environments are required.

Recent studies suggest that the structural regularity of tunnels can be exploited to improve navigation robustness. Geometry-aware approaches that align motion with the spatial constraints of the environment offer improved stability, even in low-visibility conditions [4]. Building on this idea, the method proposed in this work uses LiDAR-based distance measurements to continuously compute a centered trajectory, enabling smooth, map-independent navigation tailored to high-fidelity data acquisition. In this sense, the proposed navigation algorithm is of the reactive type [18, 19].

The three-dimensional reconstruction of tunnel geometry can support automated inspection processes in railway infrastructure. This article presents a methodology that integrates UAV-based photogrammetry with autonomous navigation, specifically designed for tunnel environments. Photogrammetry represents an innovative solution for inspection tasks in tunnel environments, overcoming limitations imposed by traditional measurement methods, such as restricted access, time constraints due to operational demands, and the lack of tools that support proper asset inspection. Using images captured by UAVs, it is possible to generate accurate three-dimensional models of tunnel geometry, including surface texture and color. These models can be integrated into virtual reality environments, enabling inspectors to perform detailed analyses of structural anomalies remotely in an immersive and precise manner. This approach significantly reduces the need for operational interruptions while enhancing safety and efficiency for inspectors, who can rely on comprehensive visual data accessible at any time. This contributes to a significant advancement in the modernization of tunnel monitoring and maintenance processes. The proposed navigation algorithm ensures the UAV remains centered within the tunnel cross-section by continuously

referencing the relative distances to the surrounding surfaces and employs a stable trajectory controller. The methodology is first validated in a simulation environment using ROS and Gazebo, followed by real-world experiments in a highway tunnel under construction. Both the simulation and physical tests demonstrated that the proposed system enables precise geometric reconstruction of the tunnel with a cross-sectional error of only 0.21%, while also capturing detailed texture and color information, highlighting the method's robustness and applicability in practical scenarios.

Therefore, the main contributions of this work are:

- Proposal and testing of an autonomous UAV navigation algorithm in an underground tunnel environment that has no bifurcations, that is, it has only one continuous section, with few or no curves.
- The proposed navigation algorithm can be used in a tunnel environment with few obstacles and overhanging structures, characterized by a practically constant cross-section along its entire length, which renders localization algorithms that utilize LiDAR scanning and point clouds impractical. These characteristics are common to rail or road transport tunnels.
- Continuous filming of the tunnel using a camera on board the drone while navigating in the center of the tunnel using the proposed navigation algorithm makes it not mandatory to obtain accurate odometry for geometry reconstruction.

In Sect. 2, the methodology for tunnel geometric reconstruction is presented, showing the UAV and its onboard sensors. The proposed navigation algorithm and the method for geometry reconstruction are described. In Sect. 3, the results and discussions are presented for both the tests of the proposed navigation algorithm for the reconstruction of tunnel geometry using computer simulations and experiments in a real tunnel. The article ends with the conclusions in Sect. 4.

2 Methodology for tunnel geometric reconstruction

This section presents the methodology for reconstructing underground tunnel geometry using photogrammetry with an RGB camera onboard a drone. Figure 2 depicts the methodology flowchart, which has the following main blocks:

- UAV flight and data acquisition: a drone with onboard sensors (LiDAR and RGB camera) must fly along the underground tunnel while filming its front view. The drone uses an autonomous navigation algorithm to fly along the tunnel center (Fig. 2a).
- Image database: the images taken with the onboard RGB camera are saved in a database. A package of images is selected from the database for processing (Fig.2b).
- Processing by the Structure from Motion (SfM) method: the set of images acquired from different observation points is analyzed to determine the camera position for each image through epipolar geometry and the

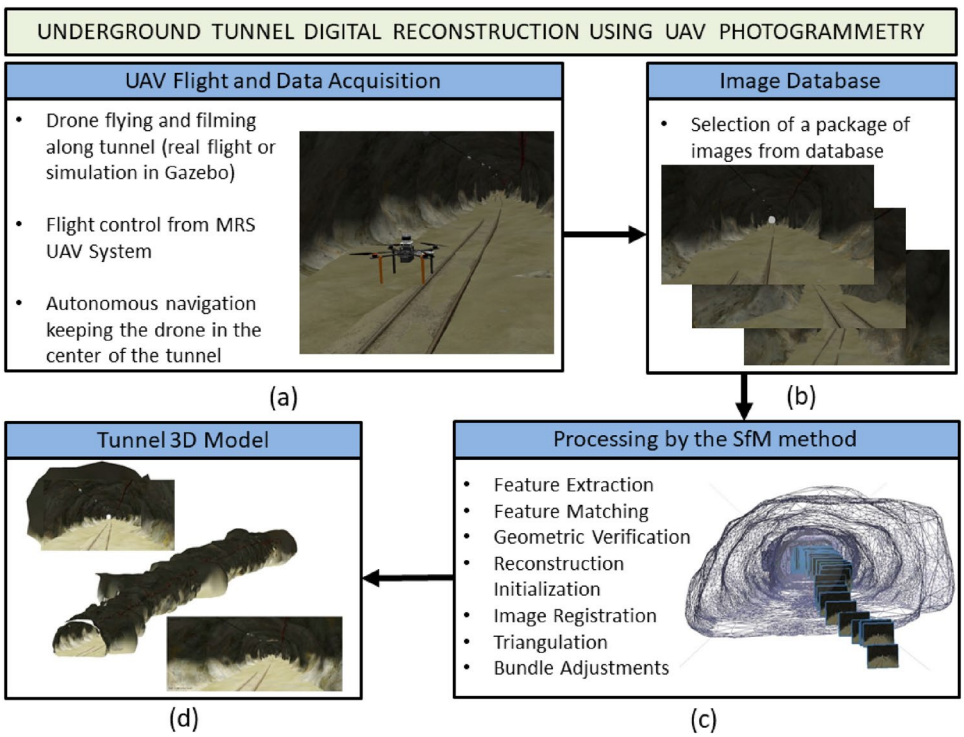

Fig. 2 Methodology created for underground tunnel geometry reconstruction using UAV photogrammetry with autonomous flight

Fig. 3 Fly4Future T650 drone digital model

(a) (b) (c)

Fig. 4 T650 drone onboard sensors, being (**a**) Ouster OS0 LiDAR sensor, (**b**) Intel Realsense D435i Depth and RGB Camera, and (**c**) GoPro Hero 10 RGB camera

subsequent reconstruction of the scene in the form of a cloud of dispersed points. Then, a sequence of steps is taken for the scene reconstruction: feature extraction, feature matching, geometric verification, reconstruction initialization, image registration, triangulation, and bundle adjustments (Fig. 2c).

- Tunnel 3D model: the result is the underground tunnel virtual 3D model (Fig. 2d).

Although the methodology is proposed for application in a real environment, such as an underground tunnel, it can also be tested in a computer simulation environment to be evaluated and improved, and its effectiveness verified quickly, with low costs and minimal risks. This way, tests in a real environment can be carried out more safely and effectively thereafter.

2.1 UAV and onboard sensors

The UAV used in this study is the Fly4Future T650, a fully autonomous and configurable platform that allows it to be programmed according to the specific requirements of each mission. Designed for heavy loads [1] with a PixHawk 6C flight controller. The onboard computing system integrates an Intel Next Unit of Computing (NUC) featuring an Intel Core i7-10710U processor and 64GB of RAM.

It features an onboard Ouster OS0 LiDAR sensor with a distance measurement range of 0.5 m to 75 m, a vertical field of view of 90° (+45° to −45°), and a 360° horizontal field, at a vertical resolution of 128 channels and horizontal resolution of 1024 points at 10 Hz. It has an Intel RealSense D435i Depth and RGB Camera positioned forward, as well as a GoPro Hero 10 RGB camera. Lastly, it also has an LED strip to improve lighting in front of the drone. The drone digital model is shown in Fig. 3, and the onboard sensors are shown in Fig. 4.

2.2 UAV autonomous navigation algorithm

This study presents an algorithm for UAV navigation in tunnels (Algorithm 1), whose objective is to determine the central axis along the tunnel, direct the UAV to navigate along this axis, and maintain its orientation in the longitudinal direction of the tunnel. A schematic view of the navigation is shown in Fig. 5.

The distances from the UAV onboard LiDAR sensor to the tunnel walls, ceiling, and floor are used to construct a three-dimensional representation of the tunnel, segmenting continuous space into structured data points. From these points, the algorithm constructs a connectivity graph that represents the navigable structure of the tunnel. Each LiDAR scan produces a local segment of points corresponding to the tunnel cross-section, which is projected based on the distance between the UAV and the obstacle. The

[1] Fly4Future, https://fly4future.com/

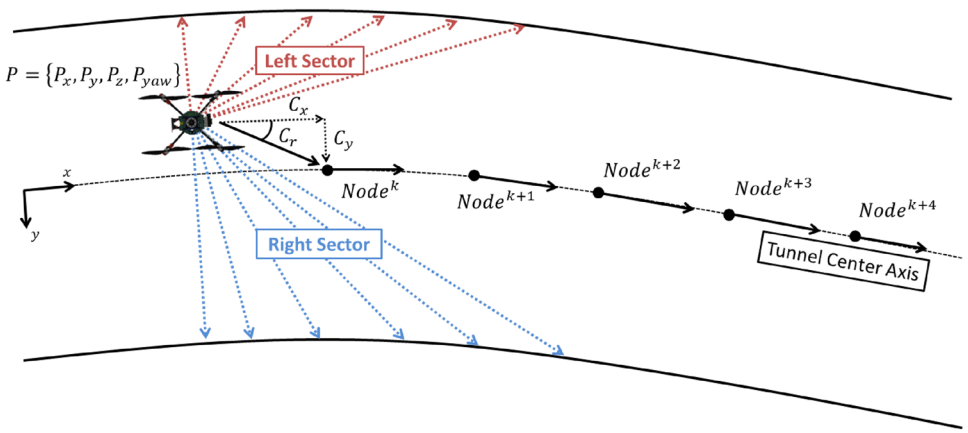

Fig. 5 Top view of a tunnel sketch. Navigation of the UAV along the tunnel and definition of the sequence of nodes. The arrows represent the onboard LiDAR, which measures the distances to the walls

algorithm clusters nearby points to extract structural features and computes their centroid positions, which are then inserted as nodes in the graph. Edges are created between consecutive nodes that satisfy distance and orientation constraints derived from the UAV's flight dynamics, ensuring that transitions correspond to feasible movements. In cases of graph construction errors, the algorithm retains prior data until sensor readings are updated, ensuring continuity and accuracy.

In the confined setting of the tunnel, where the UAV's frontal view remains unobstructed, LiDAR is particularly effective for precise distance measurement and obstacle detection, providing reliable spatial data independent of external conditions. Unlike sensor fusion, which combines multiple sensors with potentially conflicting inputs in low-light conditions, LiDAR's broad range and high data fidelity enable detailed mapping without the need for additional sensors.

The navigation algorithm constructs a connectivity graph from the discretized tunnel representation, where the graph nodes represent spatial positions, and edges define feasible transitions based on flight constraints. The algorithm strategically adds nodes along the tunnel's central axis to generate a centered trajectory while maintaining enough connections for smooth navigation.

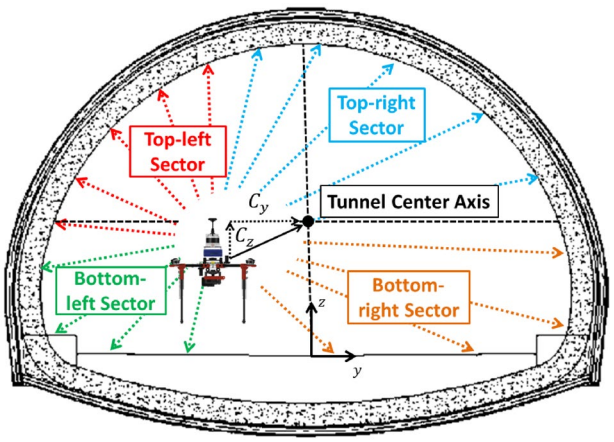

Fig. 6 Navigation algorithm, tunnel cross-section sectors

Require:
UAV position $P = \{P_x, P_y, P_z, P_{\text{yaw}}\}$
Point Cloud P_c
Tunnel Length T_l
$L_y \leftarrow \{(P_c, P_y) \mid P_c < P_y\}$
$L_z \leftarrow \{(P_c, P_z) \mid P_c < P_z\}$
$H_y \leftarrow \{(P_c, P_y) \mid P_c > P_y\}$
$H_z \leftarrow \{(P_c, P_z) \mid P_c > P_z\}$
while $P_x < T_l$ **do**
  $C_x = P_x + 2$
  $C_y = \frac{\mu(L_y)+\mu(H_y)}{2}$
  $C_z = \frac{\mu(L_z)+\mu(H_z)}{2}$
  $P'_{\text{yaw}} = \text{atan2}(C_y - P_y, C_x - P_x)$
  $C_r = P'_{\text{yaw}} - P_{\text{yaw}}$
  move_uav(C_x, C_y, C_z, C_r)
end while

Algorithm 1 UAV Autonomous Navigation Algorithm

The Y and Z coordinates of the following nodes are determined using Eq. 1, ensuring that the UAV remains centered in the tunnel. The rotation is computed using Eq. 2, which guides the UAV toward the tunnel central axis. The X position advances by 2 m from the current location, providing sufficient time for the UAV to compute the next node. However, the trajectory is continuously updated as new Y and Z positions are recalculated, meaning the UAV may adjust its path before completing the full 2-meter segment. The sequential advance of 2 m was defined through tests of the navigation algorithm in the simulation environment, where the value of 2 m indicated navigation with smooth and continuous advance, avoiding intermittent pauses and oscillations in the movement.

$$C_{y|z} = \frac{\mu(L_{y|z}) + \mu(H_{y|z})}{2} \tag{1}$$

$$C_r = \text{atan2}\left(C_y - P_y, C_x - P_x\right) \tag{2}$$

In this equation, μ represents the average value. $L_{y|z}$ and $H_{y|z}$ correspond to the values lower and higher than the UAV position on the corresponding axis, respectively. $C_{y|z}$ defines the central nodes, which guide the next position of the UAV along Y or Z, while C_r determines the necessary rotation to keep the UAV aligned with the trajectory. P_x, P_y, P_z, and P_{yaw} represent the UAV's current position in X, Y, Z and yaw orientation.

To compute $L_{y|z}$ and $H_{y|z}$, the graph is segmented based on the nodes' relative position to the UAV along the axis of interest. $L_{y|z}$ includes nodes with values smaller than the UAV's current position, while $H_{y|z}$ contains larger values. Figure 6 illustrates these variables within the tunnel, where the top-left and top-right sectors correspond to H_z, the top-right and bottom-right sectors represent H_y,

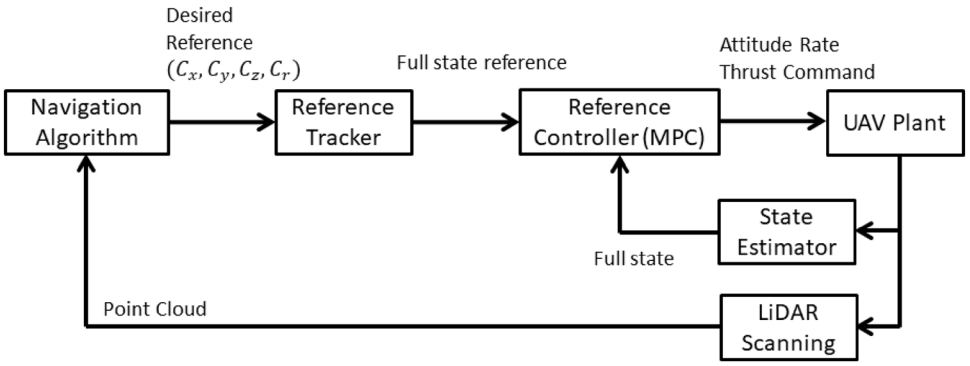

Fig. 7 Navigation and control system architecture.

the bottom-right and bottom-left sectors correspond to L_z, and the bottom-left and top-left sectors represent L_y. Additionally, Fig. 5 depicts the UAV navigating a curved tunnel, following the future center nodes while considering the left and right sectors. As this is a bidirectional example, the *Z*-axis is not considered.

As the UAV moves, new LiDAR frames continuously update this graph: when new nodes fall near existing ones, the position is merged to refine the map, while outdated or inconsistent nodes are gradually pruned. This dynamic process ensures that the graph remains geometrically consistent and computationally efficient even under sensor noise or partial occlusion.

This approach enhances efficiency by ensuring the UAV continuously follows the tunnel center adaptively. By maintaining a consistent strategy across both axes, the algorithm avoids unnecessary re-evaluations and adapts smoothly to the tunnel shape [4]. The process continues until the predicted tunnel length is covered.

The UAV algorithm selects the path closest to the tunnel center at intersections, aligning with its goal of maintaining a central trajectory. This straightforward approach is practical given that the algorithm is primarily designed for single-path tunnels with minimal intersections, allowing it to manage these cases without complex intersection-handling mechanisms.

The navigation algorithm provides the reference of the local position in 3D coordinates and heading (C_x, C_y, C_z, C_r) sequentially to the UAV reference tracker, as shown in Fig. 7, which computes a feasible, smooth, and evenly sampled full-state control reference to the reference controller. In the presented work, we utilized the controller applied in the autonomous navigation MRS UAV System of the T650 drone, which employs linear model predictive control (MPC), as described in [20, 21].

The UAV navigates by continuously adjusting its orientation based on real-time observations rather than relying on a fixed position estimate. This enables it to follow the tunnel path smoothly, even in turns, without requiring precise global positioning estimated from SLAM odometry, which can be unreliable in featureless tunnel environments. The UAV aligns its forward view with the tunnel path while maintaining a centered trajectory by continuously adjusting its orientation based on real-time observations. This adaptive approach ensures stable navigation even in complex and dynamic tunnel structures.

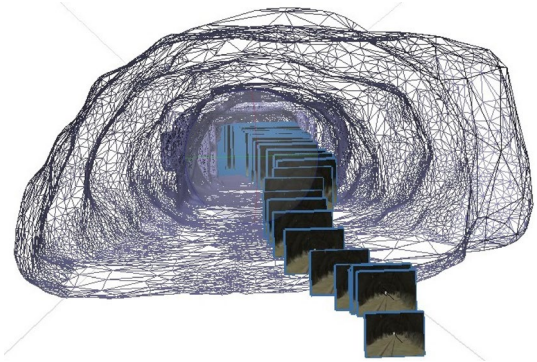

Fig. 8 Camera position for each image and the subsequent reconstruction of the scene in the 3D form

2.3 Selection of images from database

The criterion for selecting images to successfully reconstruct the 3D model of the tunnel from the package of images obtained from real flight or the simulation is to select as few images as possible that maintain at least 70% overlap between two successive images.

2.4 3D reconstruction based on photogrammetry SfM

With the assistance of the Argisoft Metashape Pro® software[2] the method known as Structure from Motion (SfM) was employed for three-dimensional reconstruction. This process involves analyzing a set of images acquired from different observation points, allowing for the determination of the camera position for each image through epipolar

[2] Argisoft Metashape Pro - https://www.agisoft.com/,

geometry and the subsequent reconstruction of the scene in the form of a cloud of dispersed points, as depicted in Fig. 8. After this initial phase, it is possible to enhance the scene representation by using a more detailed and dense reconstruction with the Multi-View Stereo (MVS) method, as described in [22].

The sequence of steps taken by SfM for the three-dimensional reconstruction of the scene is presented as follows:

1. Feature Extraction: A scan is performed on the images to find points with distinctive characteristics, such as shape, color, or texture, which serve as anchor reference points in other images.
2. Feature Matching: This step seeks points corresponding to the anchor points in other partially overlapping images. Images with more matches represent the same scene in different images.
3. Geometric Verification: The correspondences found in the previous step only ensure that two distinct images have similar points. Finding the geometry that maps the correspondence with the highest number of common points between distinct images is necessary. The confidence level computation uses Eqs. (3) and (4).
4. Reconstruction Initialization: This is an important phase in the reconstruction, as it determines the location where the highest number of verified geometries is found. The more verified geometries there are, the better defined the scene of the reconstructed model becomes.
5. Image Registration: It is necessary to calculate the camera pose (position and rotation) for each newly incremented image, considering the 3D points found in the reconstruction initialization. To estimate the camera pose in coordinates, it is necessary to define six degrees of freedom (inclination, rotation, and yaw axes) by the Perspective-n-Point (PnP) problem equation.
6. Triangulation: A triangulation process defines the 3D coordinates of new points that can be added to the reconstruction and thus generate a denser point cloud. This triangulation is performed with epipolar geometry, carries intrinsic position errors from the previous step. It can calculate the coordinates of epipolar lines that do not correspond with the surface, generating reprojection errors.
7. Bundle Adjustments: To minimize the position errors generated by epipolar reprojection, adjustments are made by applying damped least-squares techniques.

Figure 9 shows the example of interaction between the images *sim_tunnel_0500* and *sim_tunnel_0650*, whereby a total of 282 homologous points were found between the images, of which 138 had their geometry validated (blue vector) and 144 invalidated (red vector).

The criteria for determining the confidence level of the result are given by,

$$CI = \mu \pm Z \frac{C_p}{\sqrt{n}} \tag{3}$$

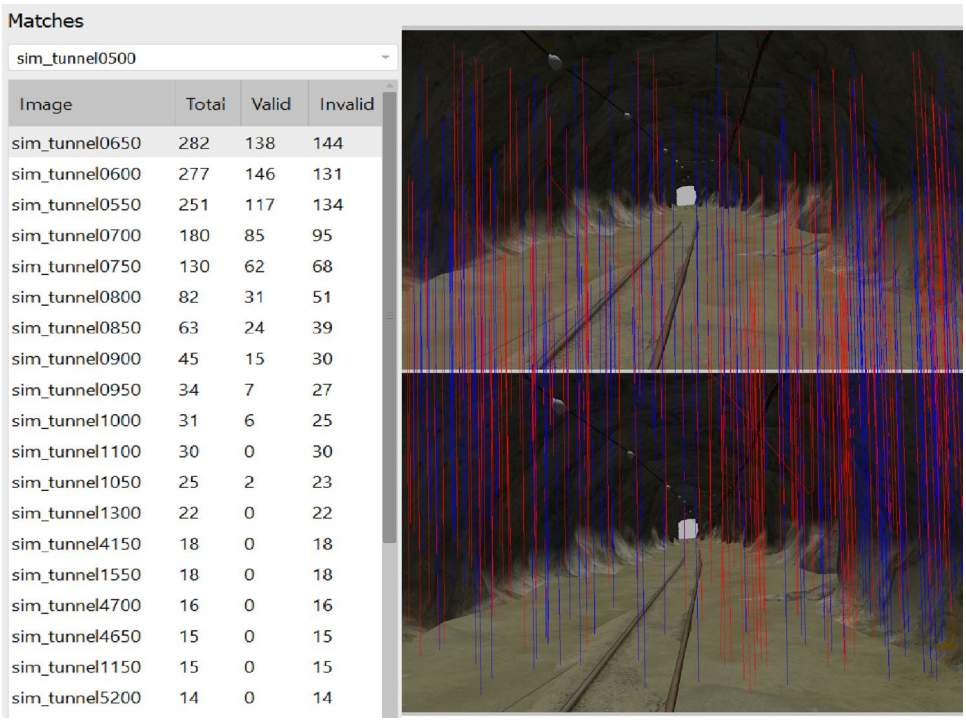

Fig. 9 Red lines correspond to the homologous points, and the blue lines represent geometries verified

Being CI, the confidence interval; μ, the population mean; $Z(95\%)$, the confidence level; n, the sample size; and C_P, the sample dispersion, defined as:

$$C_P = \begin{bmatrix} \sigma_x^2 & \sigma_{xy} & \sigma_{xz} \\ \sigma_{yx} & \sigma_y^2 & \sigma_{yz} \\ \sigma_{zx} & \sigma_{zy} & \sigma_z^2 \end{bmatrix} \tag{4}$$

While σ_x^2, σ_y^2, and σ_z^2 are the variances in the x, y, and z directions, respectively, indicating the uncertainty (or dispersion) of the position estimates in these directions. The components σ_x, σ_y and σ_z of the tensor, where $i \neq j$, represent three-dimensional covariances in the x, y, and z directions. These variables indicate how one direction is associated with variations in another direction. In the context of validating homologous points in Agisoft Metashape, these elements help to understand the interdependence of displacements, contributing to a more accurate analysis of the 3D reconstruction.

The model was quantitatively evaluated using Root Mean Square (RMS) error. In the photogrammetric context, RMS refers to the average reprojection error, that is, the difference between: The position where the point was observed in the image, and the position where the same point should appear according to the calculated geometry (camera model and point cloud). Mathematically:

$$RMS = \sqrt{\frac{\sum \left[(x_i - \hat{x}_i)^2 + (y_i - \hat{y}_i)^2\right]}{N}} \tag{5}$$

where x_i and y_i are the observed coordinates and $\hat{x}_i$, $\hat{y}_i$, are the reprojected coordinates, and N is the number of tie points.

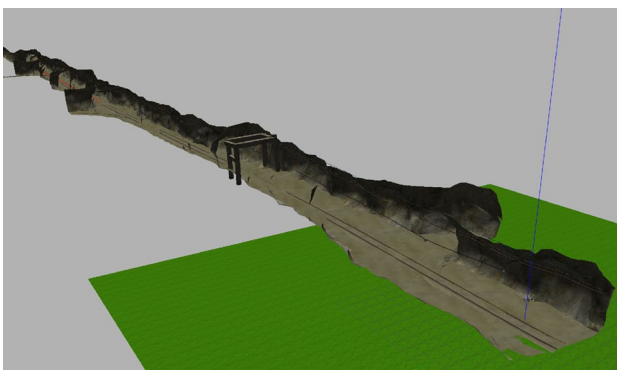

Fig. 10 Visualization of the reference tunnel model used in the simulation in Gazebo

3 Results and discussion

Evaluation of the proposed methodology and navigation algorithm started within a simulated environment due to the time-consuming, expensive, and risky nature of applying, testing, and refining the methodology in real-world underground tunnel scenarios with drones. This decision enables a gradual and cost-effective validation process, enhancing safety while facilitating rapid iteration and improvement of the methodology. The methodology and navigation algorithm were tested in a real-world underground tunnel scenario in the second phase.

3.1 Simulation environment

The simulation environment for the UAV flights utilized the Multi-Robot Systems (MRS) UAV System,[3] as detailed in [20]. This system is based on the Robot Operating System (ROS)[4] utilizing the Noetic version, as its middleware robotics framework [23], and is seamlessly integrated with the Gazebo open-source robotics simulator [24].

The MRS system employs a Software-in-the-Loop (SITL) approach, whereby the UAV-embedded software components are simulated in a virtual environment, enabling comprehensive testing and validation without reliance on physical hardware. This approach not only facilitates the assessment of system functionality, algorithm performance, and overall system behavior in a controlled and efficient manner but also provides the flexibility to seamlessly transition and utilize the same software components for real-world flights when needed.

The simulator incorporates controller algorithms, specifically employing Model Predictive Control (MPC) [25], and Simultaneous Localization and Mapping (SLAM) methods, with Octomap [26] being utilized in our case. These algorithms are not limited to simulation; they can be seamlessly applied to real UAVs using the SITL approach, ensuring consistency between simulation and real-world scenarios.

A segment was selected from the three-dimensional model of the historically significant Edgar research mine [5] in Idaho Springs, Colorado [27, 28] to assess the tunnel geometry reconstruction methodology. This virtual representation faithfully replicates the complexities found in underground mine environments, incorporating variations in tunnel widths, irregular surfaces, and elevation changes. The chosen excerpt, depicted in Fig. 10, spans approximately 250 ms, providing a representative and challenging

[3] MRS UAV System - https://github.com/ctu-mrs/mrs_uav_system

[4] ROS - https://www.ros.org/,

[5] Edgar Mine [27]

scenario to effectively assess the algorithm's ability to navigate and accurately reconstruct diverse tunnel geometries.

The simulation takes place under ideal conditions, being that its environment has no wind and lacks lighting sources, such as lamps, and only includes the color of the walls. This simplification, compared to the real environment, facilitates the acquisition of clear images throughout the drone flight within the simulated tunnel.

3.2 Testing the methodology and autonomous navigation algorithm using data acquisition from simulation

The real-time simulation allows visualizing the drone flight within the underground tunnel using the Gazebo software environment, as depicted in Fig. 11. Additionally, Fig. 12 illustrates the simulation visualization in RViz, a 3D visualizer designed for ROS [29]. RViz showcases the drone model position, orientation, current motion command, and onboard sensor data, including markers representing LiDAR distance measurements in a point cloud and visualizations from the RGB and depth cameras.

During the flight simulation along the underground tunnel, images from the onboard RGB camera are saved in PNG format at 30 frames per second, from the drone's takeoff at the tunnel entrance to landing after covering the entire tunnel. Using the previously described criteria of at least 70% overlap between successive images, a package of 122 images from the onboard RGB camera visualization database is selected for post-processing to create a virtual geometry reconstruction of the underground tunnel section of the Edgar research mine. Thus, once the geometry is reconstructed, it can be compared with the original three-dimensional geometry file of the underground tunnel to verify the effectiveness of the reconstruction methodology from the images.

The drone flying inside the underground tunnel model section was simulated using the autonomous navigation algorithm presented. It aimed to keep the drone centered in the tunnel section while gradually moving forward, simultaneously filming its front view using the onboard Realsense D435i Depth and RGB camera. The selected package of images was saved and post-processed using the 3D reconstruction methodology based on the photogrammetry SfM described previously, resulting in a reconstructed version in a PSX file.

The reconstructed model is shown in Fig. 13, where the confidence model represents the regions of the map with the highest or lowest number of images whose homologous points were validated according to the likelihood criteria. The color scale presents a confidence model with approximately 55,000 vertices with continuous classification. Let P

Fig. 11 Simulation visualization in Gazebo of Fly4Future T650 drone flying inside the underground tunnel

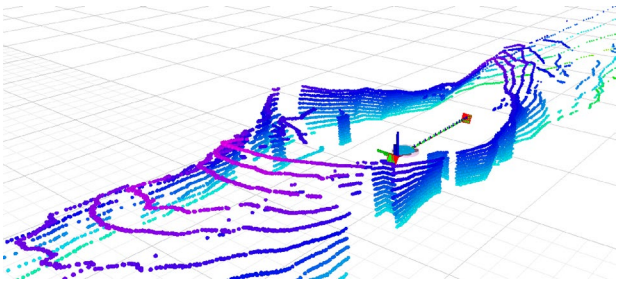

Fig. 12 Simulation visualization in RViz software of Fly4Future T650 drone flying inside an underground tunnel

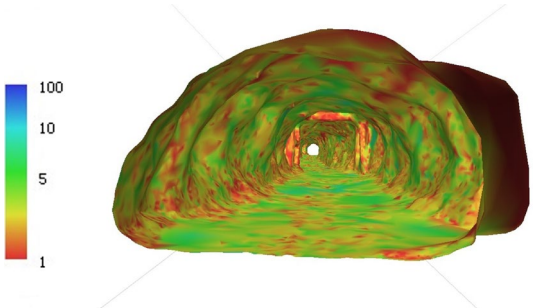

Fig. 13 Outcome of the 3D reconstruction, confidence model

be any point, position P is validated with 95% confidence when its variation is less than the acceptance threshold defined by the operator. It then receives a blue vector if the variation is more significant than the acceptance criterion defined by the operator, and receives a red vector when the position is not validated, as shown in Fig. 9. The color of the confidence map shifts towards blue as more images where point P appears are validated, indicating the region with the highest number of images within the confidence interval (CI). A consistent pattern of interactions is generally observed across the walls, ceiling, and floor, potentially attributable to two factors:

1. The saturation of the lighting distributed in two parts means that the Argisoft® SfM algorithm was able to partially find the stereocorrelation between homologous points in different images, discarding the points in the images that do not fit the invariance criterion scale location.
2. The displacement of the UAV in the longitudinal direction, navigating with the autonomous flight algorithm, maintained equidistance to the walls of the FOV (Field of View). The image capture angle of the field of view is horizontal at 87° and vertical at 58° for the camera used.
3. Following this configuration defines the maximum range of the edges of the image as a function of the distance to the target, ensuring navigation in the center of the tunnel while maintaining an equal distribution of confidence

Adjustments are necessary to enhance reliability, but may increase execution time and the volume of collected data.

Figure 14 illustrates the UAV trajectory influence of image acquisition positions with overlap assurance. The images in the center, shown in blue and aligned with the image acquisition direction, exhibit the highest overlap assurance, with more than nine overlapping images. As one moves towards the edges, the overlap assurance gradually decreases until it reaches red, where overlap occurs with only one other image.

Lastly, Fig. 15 depicts the outcome of the three-dimensional model of the tunnel, showcasing details in texture, shape, and color, faithfully reproducing the initial virtual model. This indicates success in the goal of 3D reconstruction of infrastructures.

3.3 Testing the methodology and autonomous navigation algorithm using data acquisition from experiments with UAV

As the underground tunnel where the experiments were carried out had little lighting, two additional sets of light-emitting diodes (LEDs), each with a power of 50 W, were added to improve the quality of the images acquired by the drone. The drone lighting system is shown in Fig. 16.

Experiments were conducted to test the methodology of geometrically reconstructing the tunnel using photogrammetry with a camera onboard a UAV. The tunnel used for the experiments was a highway tunnel under construction in the city of São Sebastião, in the state of São Paulo, Brazil, whose location is shown in Fig. 17. Figure 18 presents the Fly4Future T650 drone inside the underground highway tunnel. This tunnel has a total length of approximately 3.0 km and a cross-section of roughly 12 m in width and 7 m

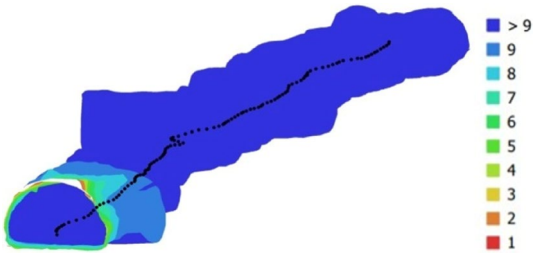

Fig. 14 Outcome of the 3D reconstruction, camera locations, and image overlap

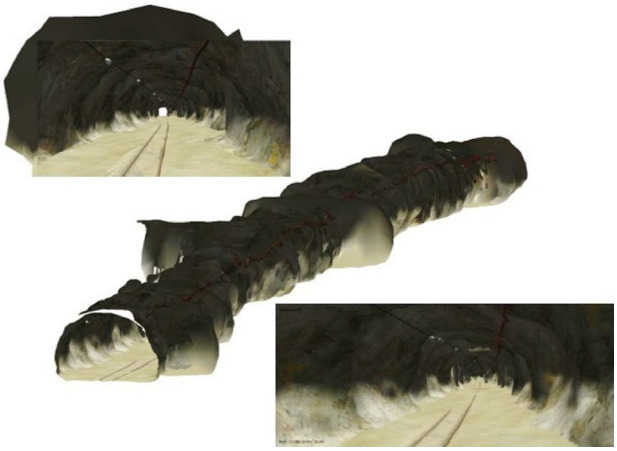

Fig. 15 Reconstructed underground tunnel 3D model textured from images acquired by computer simulation in the Gazebo environment

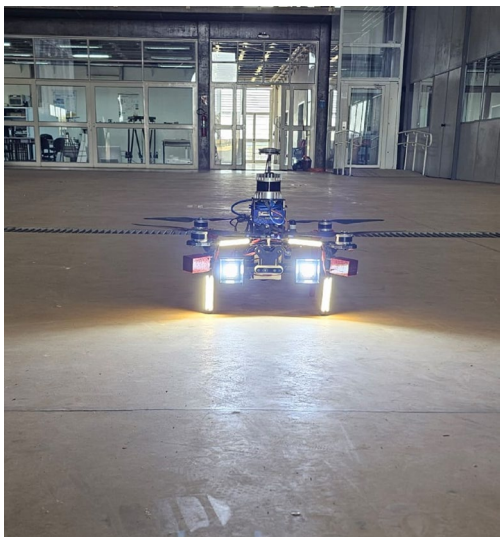

Fig. 16 Improvement of the drone's lighting system by adding two more sets of LED

in height. However, due to ongoing construction activities, including the constant movement of workers and vehicles, the experiments were conducted in sections of approximately 200 m in length.

Fig. 17 Location of the underground highway tunnel under construction, in the city of São Sebastião, State of São Paulo, Brazil

Fig. 18 Experiments for underground tunnel reconstruction using photogrammetry

Table 1 Video specification of cameras

Camera	Video Resolution	Frame rate (fps)
GoPro Hero 10	8MP (3840x2160 pixels)	30
Realsense D435i	1MP (1280x720 pixels)	10

Video recordings of sections of the highway tunnel were conducted using two cameras onboard the drone: GoPro Hero 10 and RealSense D435i. The video capturing specifications are detailed in Table 1.

The Intel RealSense D435i camera was configured to operate at 1 MP and 10 FPS based on the specific characteristics of the testing environment and the need to optimize post-processing. In indoor settings with low lighting, higher resolution introduces noise without providing significant benefits [30], whereas lower resolution enhances the quality of processed data. Furthermore, this configuration reduces the collected data volume, streamlining processing and increasing the system's overall efficiency. This is particularly important because images from this camera are processed and recorded by the computer on board the drone (Intel NUC). Therefore, the data file saved from the experiment is synchronized with the drone flight data from the controller board (Pixhawk 6C) and the point cloud data obtained by the LiDAR sensor.

Since the GoPro Hero 10 camera was not connected to the drone's onboard computer, its recording resolution could be higher–set to 8MP- with files stored on the camera's microSD card. Figure 19 presents video frames from the (a) GoPro Hero 10 and (b) Intel Realsense D435i, showing that the GoPro camera produces significantly clearer images with more details of the tunnel.

Both cameras recorded videos through autonomous drone flights using the proposed navigation algorithm. The

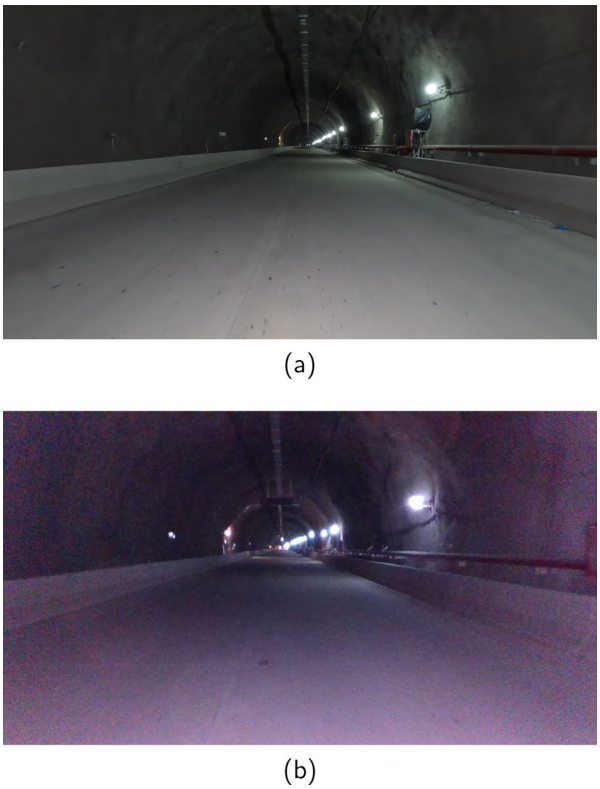

Fig. 19 Video frames from cameras onboard UAV: (**a**) GoPro Hero 10. (**b**) Intel Realsense D435i

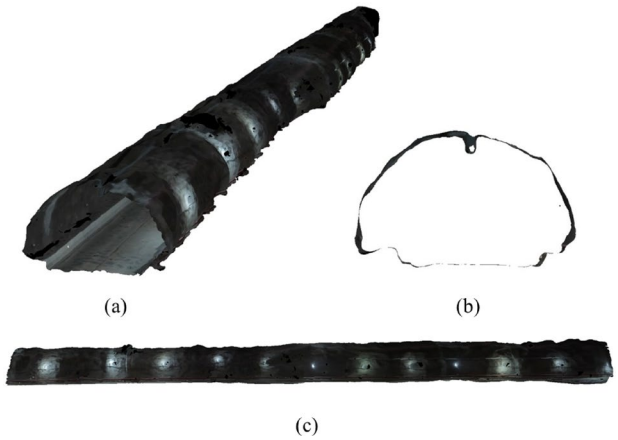

Fig. 20 Reconstructed underground highway tunnel under construction. UAV Onboard camera: GoPro Hero 10. In (**a**) isometric view, (**b**) front view, and (**c**) side view

goal was to keep the drone aligned with the tunnel walls and maintain a centered position while navigating.

A challenge encountered was calculating the drone odometry. Due to the tunnel having a nearly constant cross-section along its entire length, the SLAM algorithm struggled to estimate the drone speed and position, as the LiDAR-generated point cloud remained almost unchanged throughout the flight. However, the LiDAR sensor could still measure distances to the tunnel walls and ceiling, allowing forward movement while avoiding obstacles.

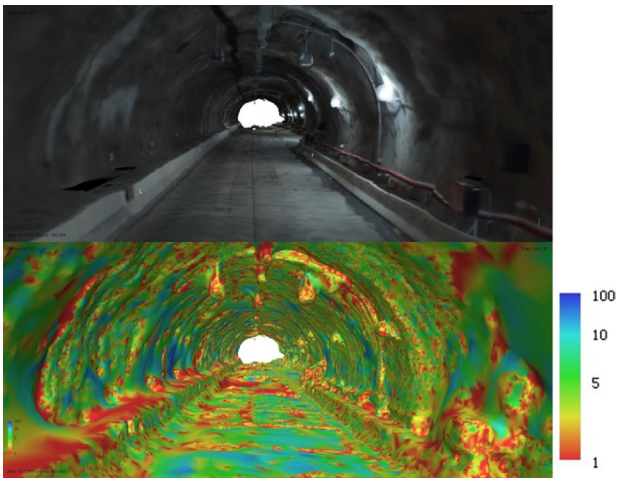

Fig. 21 Confidence map of the photogrammetry model. UAV Onboard camera: GoPro Hero 10

Table 2 Summary of qualitative evaluation

Color	Pixel Percentage (%)	Confidence Level	Estimated GSD (cm)
Red	14.40	Low	7.5
Yellow	70.20	Moderate	4.5
Green	14.90	High	3.0
Blue	0.50	Higher	1.5

Despite these challenges, the drone successfully navigated a 200-meter stretch in 96 s, achieving an average speed of 2.08 m/s. The images captured by the GoPro Hero 10 were then used for the 3D reconstruction of the tunnel section, employing the same photogrammetry methodology described earlier. Fig. 20 presents views of the resulting 3D model.

The quality of the photogrammetric model was assessed by analyzing the confidence map histogram (Fig. 21) and pixel distribution. This provides a visual representation of the accuracy and reliability of the 3D reconstruction. In the confidence map, colors represent different levels of confidence, that also relate to the ground sample distance (GSD), which represents the resolution level of the 3D model, as summarized in Table 2:

1. Red: Low confidence–potentially due to missing data or issues during image capture.
2. Yellow: Moderate confidence–reasonable data coverage but not optimal.
3. Green: High confidence–accurate and reliable reconstruction.

4. Blue: Very high confidence–ensuring precise reconstruction.

The confidence map analysis showed a varied confidence distribution across the reconstructed areas. Low-confidence regions, representing 14.4%, were likely caused by poor lighting, occluded points, or vertical oscillations, which affected data recovery and model quality. Conversely, the majority of the area, representing 70.2%, exhibited moderate confidence, indicating reasonable but suboptimal data quality. This suggests that while image capture was effective, some limitations impacted reconstruction accuracy. High-confidence regions, representing 14.9%, confirmed an accurate and reliable reconstruction, although they covered a smaller area than the moderate-confidence regions. Finally, very high-confidence areas, represented by 0.5%, were minimal, suggesting that few regions achieved near-perfect reconstruction.

The quantitative comparison of the tunnel cross-section was carried out by overlaying the original design (gray) and photogrammetric model (red), derived from the methodology employed in this work, as shown in Fig. 22.

This analysis revealed a difference of 0.21%, with the designed area measuring 70.72 m^2 and the area obtained by the photogrammetric model measuring 70.57 m^2. This slight discrepancy suggests that, despite the areas of low confidence, the model can capture geometric features with high accuracy in terms of cross-sectional area.

Figure 23 shows the spatial distribution of tie points along the tunnel axis as a function of the distance between consecutive image pairs. Approximately 55% of all tie points were generated within 50 m, while 28% were obtained up to 100 m, 10% up to 200 m, and only 7% beyond this distance.

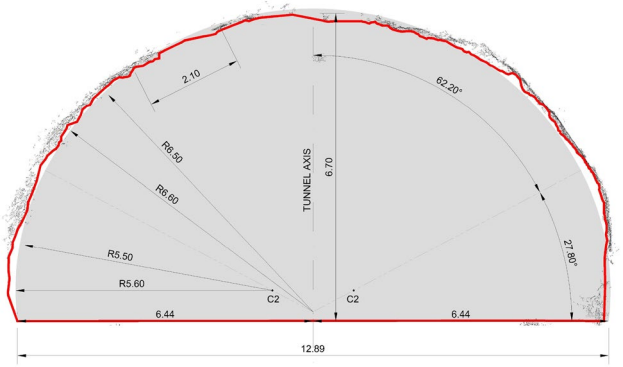

Fig. 22 Tunnel cross-section design in grey, and 3D photogrammetric model in red

This concentration of correspondences at shorter baselines indicates that the image overlap and camera field of view (FOV) were optimal within this range, ensuring sufficient redundancy and geometric stability for the 3D reconstruction. As the inter-image distance increases, a progressive decrease in the number of valid correspondences is observed, reflecting both the reduction in overlap and the increase in angular difference between successive captures. Moreover, the comparison between validated (blue) and invalidated (orange) tie points reveals a clear trend of performance degradation. Approximately 73% of the images acquired within 50 m showed more than half of the tie points validated, whereas only 50% of the images with inter-distances up to 100 m maintained this ratio. This behavior is strongly associated with the illumination distribution inside the tunnel, since areas with more homogeneous lighting provide higher contrast and better feature detection. The correlation between the validation rate and the zones of effective lighting confirms that texture richness, contrast, and uniform

Fig. 23 Tie point statistic

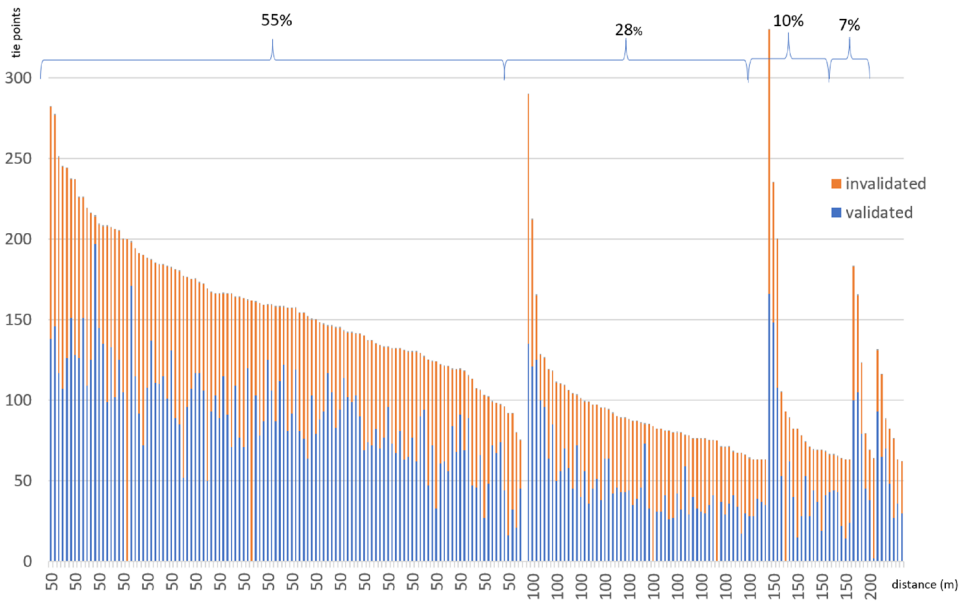

illumination are critical for robust feature matching in underground photogrammetric surveys. Consequently, the effective photogrammetric baseline of this dataset can be considered to extend up to approximately 100 m, beyond which both the geometric consistency and photometric reliability of the tie points tend to deteriorate.

The tie point statistic exported from Metashape is shown in Fig. 23, indicating direct variations between the number of matches and the average RMS error per image, defined in Eq. (5). Images with a higher match density (>100 points) had an RMS error of less than 1 px, a typical characteristic of a surface with good texture and homogeneous lighting. In contrast, pairs with fewer than 40 matches exhibited an RMS error exceeding 2 px, which is typically associated with adverse capture conditions, such as low lighting, smooth surfaces, or extreme angles of incidence. This quantitative relationship between texture, lighting, and photogrammetric matching reinforces the influence of the image's radiometric properties on the accuracy of the 3D model.

Therefore, the tunnel section was reconstructed using the proposed methodology and the autonomous navigation algorithm, enabling the acquisition of the cross-sectional geometry along its length. This data can be inspected and compared against the design specifications. However, details of internal components can still be enhanced by capturing higher-resolution images and integrating a more powerful lighting system into the drone. These refinements will enhance the final model, supporting the development of digital twins.

4 Conclusion

This paper presented a methodology for digitally reconstructing an underground tunnel geometry using photogrammetry while autonomously flying a UAV guided by the proposed autonomous navigation algorithm. This algorithm is suitable for tunnels that have no bifurcations, i.e., those with only one continuous section, with few or without curves. The proposed navigation algorithm can be used in a tunnel environment with few obstacles and overhanging structures, characterized by a practically constant cross-section along its entire length, which renders localization algorithms that utilize LiDAR scanning and point clouds are impractical. These characteristics are common to rail or road transport tunnels. The methodology and navigation algorithm were tested in a computer simulation using the MRS UAV System, ROS, and the Gazebo simulator. A digital model of a section of the Edgar Research Mine tunnel served as a reference for underground tunnel testing. The results demonstrated that the proposed methodology successfully digitally reconstructed the tunnel section, faithfully replicating details in texture, shape, and color.

Subsequently, real-world experiments were conducted in sections of a highway tunnel under construction to validate the methodology and UAV navigation algorithm for 3D geometric reconstruction via photogrammetry. The tunnel geometry was reconstructed using images captured by a GoPro Hero 10 camera.

A quantitative assessment of the cross-sections showed a 0.21% area difference between the designed (70.72 m^2) and the photogrammetric model (70.57 m^2), indicating that the methodology effectively captures geometric features. The areas of lower confidence did not significantly impact overall accuracy. A qualitative analysis further confirmed that the model reliably represents textures and colors, enhancing its fidelity. The root-mean-square error (RMS) analysis demonstrated a consistent quantitative basis for confirming the reliability of the 3D reconstruction, being that approximately 73% of the images acquired within 50 m showing more than half of the tie points validated. In contrast, only 50% of the images with inter-distances up to 100 m maintained this ratio. This behavior is strongly associated with the illumination distribution inside the tunnel, since areas with more homogeneous lighting provide higher contrast and better feature detection.

The reconstruction results in the simulated environment were superior to those in the real-world experiments. Challenges encountered in real conditions included wind currents, low lighting, and difficulties with the SLAM algorithm in odometry estimation due to the tunnel's nearly constant cross-section along its length. However, the application of the proposed navigation algorithm was still able to keep the UAV's flight in a centered position along the tunnel to perform the filming.

Further improvements can be achieved by acquiring higher-resolution images and incorporating a more powerful lighting system into the drone to capture clearer details. The installation of a drone indoor positioning system inside the tunnel, utilizing UWB (Ultra Wideband) technology, is under development to overcome the difficulties encountered in calculating odometry during flight. The resulting model can verify and compare design geometry via a digital twin, facilitating long-term monitoring of the underground tunnel's stability and structural integrity.

These findings underscore the potential of the proposed methodology and UAV autonomous navigation algorithm for accurate, rapid, and safe digital reconstruction of underground tunnels. This approach enables precise verification and comparison of design geometries through digital twins, contributing to continuous monitoring and assessment of tunnel stability and integrity. It demonstrates the robustness of the methodology in real-world applications.

Acknowledgements The authors would like to thank the support of the University of São Paulo, the Federal University of São Carlos, the São Paulo Research Foundation (FAPESP) Grant 2023/05124-1, National Council for Scientific and Technological Development (CNPq) Grant 306379/2021-0, Cathedra Under Rail, the Foundation for the Technological Development of Engineering (FDTE) and the Coordination for the Improvement of Higher Education Personnel (CAPES) Grant 88887839293/2023-00 for developing this paper.

Data Availability The data that support the findings of this study are not openly available due to reasons of sensitivity and are available from the corresponding author upon reasonable request.

Declarations

Conflict of interest The authors declare no relevant financial or non-financial interests.

References

1. Fujino Y, Siringoringo D (2020) Recent research and development programs for infrastructures maintenance, renovation, and management in Japan. Struct Infrastruct Eng 16(1):3–25
2. Mao D, Nilsen B, Feng S, Zhao H, Lu M (2015) A case study of tunnel instability in weakness zone containing swelling clay. Professor Ming Lu, Nanyang Technological University Dr. Oskar Sigl, Geoconsult Asia Singapore PTE Ltd. Dr. GuoJun Li, Singapore Metro Consulting Eds, ECI Symposium Series
3. Montero R, Victores JG, Martínez S, Jardón A, Balaguer C (2015) Past, present and future of robotic tunnel inspection. Autom Constr 59:99–112. https://doi.org/10.1016/j.autcon.2015.02.003
4. Zhang R, Hao G, Zhang K, Li Z (2023) Unmanned aerial vehicle navigation in underground structure inspection: A review. Geol J 58(6):2454–2472
5. Szrek J, Wodecki J, Błażej R, Zimroz R (2020) An inspection robot for belt conveyor maintenance in underground mine-infrared thermography for overheated idlers detection. Appl Sci 10(14):4984
6. Li Y, Xiao Z, Li J, Shen T (2024) Integrating vision and laser point cloud data for shield tunnel digital twin modeling. Autom Constr 157:105180
7. Chu H, Cao R, Deng L (2023) A collaborative inspection system composed of quadruped and flying robot for crack segmentation in tunnel environment, pp. 2406–2413. CRC Press, Boca Raton. https://doi.org/10.1201/9781003348030-289
8. Aspert N, Santa-Cruz D, Ebrahimi T (2002) Mesh: measuring errors between surfaces using the hausdorff distance. Proc IEEE Int Conf Multimed Exp 1:705–7081. https://doi.org/10.1109/ICME.2002.1035879
9. Aber JS, Marzolff I, Ries JB (2010) Chapter 3 - photogrammetry. In: Aber JS, Marzolff I, Ries JB (eds) Small-format aerial photography. Elsevier, Amsterdam, pp 23–39. https://doi.org/10.1016/B978-0-444-53260-2.10003-1
10. Chang Y, Cheng Y, Manzoor U, Murray J (2023) A review of uav autonomous navigation in gps-denied environments. Robot Auton Syst 170:104533. https://doi.org/10.1016/j.robot.2023.104533
11. Nex F, Armenakis C, Cramer M, Cucci DA, Gerke M, Honkavaara E, Kukko A, Persello C, Skaloud J (2022) Uav in the advent of the twenties: Where we stand and what is next. ISPRS J Photogramm Remote Sens 184:215–242. https://doi.org/10.1016/j.isprsjprs.2021.12.006
12. Lu Y, Xue Z, Xia GS, Zhang L (2018) A survey on vision-based uav navigation. Geo-spatial Inform Sci 21(1):21–32. https://doi.org/10.1080/10095020.2017.1420509
13. Chang Y, Cheng Y, Manzoor U, Murray J (2023) A review of uav autonomous navigation in gps-denied environments. Robot Auton Syst 170:104533
14. Ma W, Fang X, Liang L, Du J (2024) Research on indoor positioning system algorithm based on uwb technology. Meas Sensors 33:101121
15. Chen P-P, Zhang K-Y, Gao S-W, Ren S-Y (2024) Uav localization with unreliable observations in hostile underground environments. J Comput Sci Technol 39(6):1401–1418
16. Elmokadem T, Savkin AV (2022) A method for autonomous collision-free navigation of a quadrotor uav in unknown tunnel-like environments. Robotica 40(4):835–861
17. Ge S, Pan F, Wang D, Ning P (2021) Research on an autonomous tunnel inspection uav based on visual feature extraction and multi-sensor fusion indoor navigation system. In: 2021 33rd Chinese Control and Decision Conference (CCDC), pp. 6082–6089. IEEE
18. Antich Tobaruela J, Ortiz Rodriguez A (2017) Reactive navigation in extremely dense and highly intricate environments. PLoS ONE 12(12):0189008
19. Prophet S, Trommer GF (2020) Reactive navigation in cluttered indoor environment for autonomous mavs. In: 2020 27th Saint Petersburg International Conference on Integrated Navigation Systems (ICINS), pp. 1–8. IEEE
20. Baca T, Petrlik M, Vrba M, Spurny V, Penicka R, Hert D, Saska M (2021) The mrs uav system: Pushing the frontiers of reproducible research, real-world deployment, and education with autonomous unmanned aerial vehicles. J Intell Robot Syst 102(1):26
21. Baca T, Hert D, Loianno G, Saska M, Kumar V (2018) Model predictive trajectory tracking and collision avoidance for reliable outdoor deployment of unmanned aerial vehicles. In: 2018 IEEE/RSJ International Conference on Intelligent Robots and Systems (IROS), pp. 6753–6760. IEEE
22. Bianco S, Ciocca G, Marelli D (2018) Evaluating the performance of structure from motion pipelines. J Imaging 4(8):98
23. Quigley M, Conley K, Gerkey B, Faust J, Foote T, Leibs J, Wheeler R, Ng A (2009) Ros: an open-source robot operating system 3
24. Koenig N, Howard A (2004) Design and use paradigms for gazebo, an open-source multi-robot simulator. 2004 IEEE/RSJ Int Conf on Intell Robots and Systems (IROS) 3:2149–21543. https://doi.org/10.1109/IROS.2004.1389727
25. Afram A, Janabi-Sharifi F (2014) Theory and applications of hvac control systems-a review of model predictive control (mpc). Build Environ 72:343–355
26. Hornung A, Wurm KM, Bennewitz M, Stachniss C, Burgard W (2013) Octomap: an efficient probabilistic 3d mapping framework based on octrees. Auton Robot 34:189–206
27. OpenRobotics: Edgar Mine Virtual STIX. Open Robotics. https://fuel.gazebosim.org/1.0/OpenRobotics/models/Edgar Mine Virtual STIX
28. Rogers J, Gregory J, Fink J, Stump E (2020) Test your slam! the subt-tunnel dataset and metric for mapping, 955–961. https://doi.org/10.1109/ICRA40945.2020.9197156
29. Kam H, Lee S-H, Park T, Kim C-H (2015) Rviz: a toolkit for real domain data visualization. Telecom Syst 60:1–9. https://doi.org/10.1007/s11235-015-0034-5
30. Zhang X, Sun Y (2023) A high quality low-light image enhancement method. In: 2023 International Conference on Image Processing, Computer Vision and Machine Learning (ICICML), pp. 228–231. https://doi.org/10.1109/ICICML60161.2023.10424804